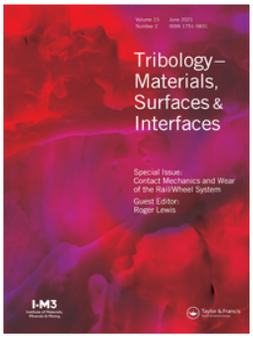

Taylor & Francis
Taylor & Francis Group

Tribology - Materials, Surfaces & Interfaces

ISSN: (Print) (Online) Journal homepage: https://www.tandfonline.com/loi/ytrb20

A vision-based approach for rolling contact fatigue evaluation in twin-disc tests on a railway wheel steel

Ileana Bodini, Candida Petrogalli, Angelo Mazzù, Simone Pasinetti, Takanori Kato & Taizo Makino

To cite this article: Ileana Bodini, Candida Petrogalli, Angelo Mazzù, Simone Pasinetti, Takanori Kato & Taizo Makino (2021) A vision-based approach for rolling contact fatigue evaluation in twin-disc tests on a railway wheel steel, Tribology - Materials, Surfaces & Interfaces, 15:2, 92-101, DOI: 10.1080/17515831.2020.1825062

To link to this article: https://doi.org/10.1080/17515831.2020.1825062

Published online: 01 Oct 2020.

TRIBOLOGY - MATERIALS, SURFACES & INTERFACES
2021, VOL. 15, NO. 2, 92–101
https://doi.org/10.1080/17515831.2020.1825062

Institute of Materials, Minerals & Mining
Taylor & Francis
Taylor & Francis Group

RESEARCH ARTICLE

A vision-based approach for rolling contact fatigue evaluation in twin-disc tests on a railway wheel steel

Ileana Bodini [a], Candida Petrogalli [a], Angelo Mazzù [a], Simone Pasinetti [a], Takanori Kato[b] and Taizo Makino[b]

[a]Department of Mechanical and Industrial Engineering, University of Brescia, Brescia, Italy; [b]Steel Research Laboratories, Nippon Steel Corporation, Amagasaki, Japan

ABSTRACT
A vision-based experimental methodology was developed for monitoring the surface state evolution of specimens during twin-disc rolling contact tests, aimed at providing information for identifying the damage phenomena. The system is based on a high-speed camera and three laser pointers for illuminating the specimen surface. Images of the specimen surface are acquired and processed, allowing the definition of synthetic surface state indexes, as well as the section profiles of the surface. The vision system was applied to alternated dry–wet rolling–sliding contact tests on railway wheel steel specimens, highlighting its effectiveness in the damage evaluation. The potential of the section profile reconstruction as a tool for surface topology analysis was shown.

ARTICLE HISTORY
Received 31 March 2019
Accepted 6 December 2019

KEYWORDS
Online monitoring; image processing; rolling contact fatigue; wear; damage assessment

1. Introduction

Twin-disc tests are an effective method for characterizing the material response to rolling–sliding. Twin-disc testing machines, which can have various configurations and sizes, are aimed at reproducing at the laboratory scale the working conditions of components subjected to contact loads: this is realized by means of two discs put in rolling and/or sliding contact on their lateral surface, keeping their axes parallel. Usually, contact load, sliding and rolling speed and torque are controlled during the tests; lubricants, friction modifiers or contaminants can be optionally added at the contact interface. Twin-disc tests are used for studying damage phenomena in various fields of application. For instance, twin-disc tests were used for studying rolling contact fatigue (RCF) in surface hardened materials, such as steels for bearings or gears [1–6]. In these cases, RCF usually develops through the nucleation and propagation of cracks from surface or subsurface defects, which lead to localized severe damage due to the removal of large material flakes. Such phenomena are usually hidden during their progress, appearing rather suddenly and determining the end of the test: in these cases, therefore, to detect the instant when the damage occurs is crucial for quantifying the specimen's life and stopping the tests for post-test analyses.

Another field where twin-disc testing is widely used is the investigation of damage occurring in wheel–rail contact. In this field, the materials are softer with respect to the previous case and the damage phenomena are rather different. Wear is usually much higher, appearing as a continuous and uniform removal of material layers from the surface; due to the high frictional forces, severe plastic flow along the friction direction occurs in the layer under the surface, leading to the formation of surface cracks [7–13]. The addition of third bodies or fluids at the contact interface changes the damage phenomenology. Solid contaminants, such as sand, oxides or wear debris, enhance high rate wear due to abrasion and increased ratcheting [7,14–16]. Grease, lubricants, friction modifiers or water, while reducing friction and wear, can promote the propagation of surface cracks by the mechanism of pressurization of the fluid entrapped inside the cracks [7,12,17–20]. In the wheel–rail contact field, the degradation of the contact surface is more progressive with respect to the field of bearings and gears; therefore, a continuous monitoring of the surface state evolution is needed for the damage assessment. However, the damage phenomena occurring in wet or lubricated contact can be rather sudden, so even in this case, a damage detection system is necessary for a reliable testing procedure.

Typically, the damage detection is carried out by means of visual inspections, e.g. the test is interrupted and observed by the naked eye for detecting spalling or pitting. Some systems also have accelerometers able to stop the tests if a threshold level of vibrations is exceeded [20,21]. The damage quantification can be obtained by means of destructive and non-destructive measurements.

CONTACT Angelo Mazzù angelo.mazzu@unibs.it

The destructive measurements consist essentially in cutting the specimens at the end of the tests, observing the subsurface microstructure and crack morphology by optical or scanning electron microscopy, and measuring the hardness on these sections or on the contact surface [1,4,6,8–15,17,19–21]. In [2], even residual stress measurements were done by means of X-ray diffraction and deep-hole drilling (DHD).

Non-destructive measurements can be periodical or continuous. Periodical techniques allow measurements during interim test stops. Among these, the most common is wear evaluation, which is obtained by specimen weighing during test stops [8–19]. This measurement gives information on the overall specimen wear. If information on local damage and surface state is needed, more sophisticated technologies are needed. Optical surface profilometers can be used for reconstructing the surface topology [3,5,7]: the procedure needs test stopping and acquisition of surface replicas which have to be displaced from the testing machine to be analysed. An alternative way for evaluating the surface damage is optical or SEM microscope observation of the specimen surface [4,8,9,11,19,20], which requires periodical specimen dismounting [21]. In [21], a procedure including even the periodical measurement of the Barkhausen noise was introduced. Continuous monitoring of surface damage is usually performed by means of online indirect measurements, such as the coefficient of friction or vibrations [9–21]. The indirect measurements (vibrations, Barkhausen noise, coefficient of friction) do not provide a univocal indication about the damage mechanism: they can be affected by various phenomena, such as wear, ratcheting, RCF, even in competition with each other. Therefore, damage monitoring requires the combination of various measurement techniques, in order to identify with more precision the damage phenomena occurring.

In this paper, the introduction of a dedicated vision-based measurement system to a twin-disc test bench for monitoring and evaluating the damage evolution is discussed. This system provides a tool for monitoring the surface state and damage, by means of techniques of image analysis giving quantitative damage indexes [22]. It is mounted on-board, therefore, in dry tests, it can be used as a continuous direct measurement system. In wet tests, owing to the water drops splashing from the contacting discs, it cannot be used online, but it allows fast periodical measurements. The information provided by the system is on a twofold level. The first level is a general quantification of the surface state based on the analysis of lights and shadows under diffused light: this will be addressed as 2D analysis in the following. The second level is a localized evaluation of the damage development in the depth, obtained by the analysis of the deformation of a light blade projected on the contact surface: this will be addressed as section profile analysis in the following. The 2D analysis was previously applied to the evaluation of wear evolution in dry contact [23]. In this paper, the system is applied to the analysis of damage in alternated dry–wet contact, where both progressive and sudden damage can occur. Furthermore, the potential of the section profile analysis as a non-destructive method for damage quantification, as well as for three-dimensional reconstruction of surface topology, is shown.

2. Testing procedure

The tests were carried out by means of the twin-disc testing machine shown in Figure 1, whose detailed description is provided in [13].

It is a twin-disc machine where the specimens are fixed to independent shafts. One of them can be displaced orthogonally to the shaft axis by a hydraulic cylinder, which applies the imposed contact load as

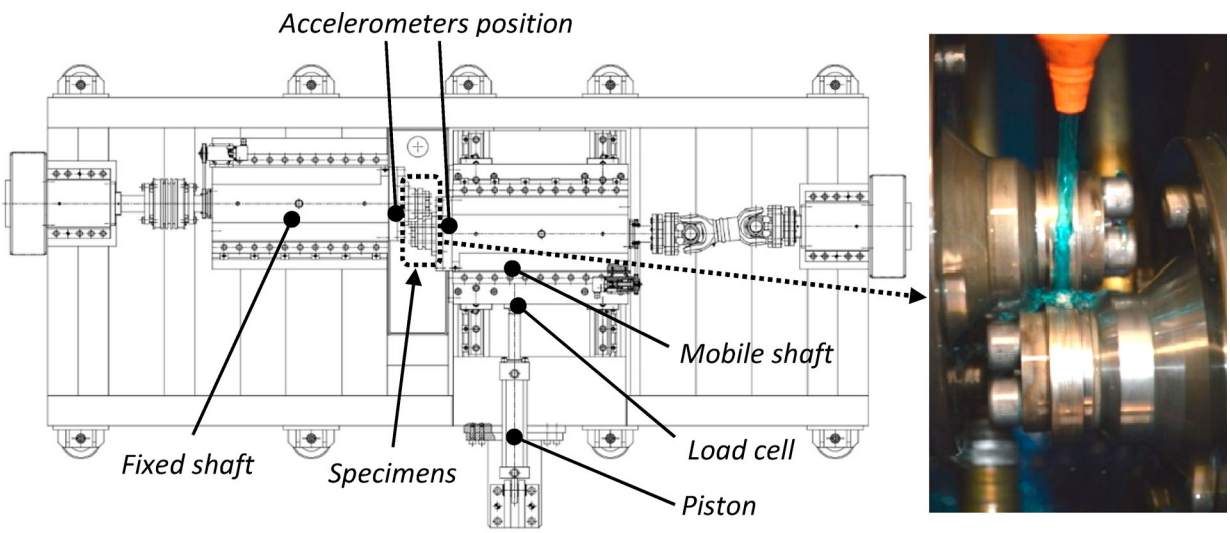

Figure 1. Schematic of the twin-disc test bench.

Table 1. Summary of the applied test conditions.

Test ID	Dry–wet sequence
T1	50,000 dry + 50,000 wet + 50,000 dry + 50,000 wet + … up to failure
T2	50,000 dry + 50,000 wet + 50,000 dry + 50,000 wet + … up to failure
T3	50,000 dry + 50,000 wet + 50,000 dry + 50,000 wet + … up to failure
T4	600,000 dry + *n* wet up to failure
T5	1,000,000 dry + *n* wet up to failure

well. The rolling speed of each shaft is measured by encoders, whereas a load cell located at the piston head measures the contact load between specimens.

Two piezo-accelerometers are mounted on the specimen supports: one on the fixed shaft in the vertical direction and the other one on the mobile shaft in the horizontal direction, both normal to the rotation axis. The transducers used are Wilcoxon 736 IEPE accelerometers, with nominal sensitivity 0.98 V/(m/s^2), full scale 5 m/s^2, linear bandwidth within the range 5–20 kHz. Rolling–sliding tests in dry and wet contact were carried out on specimens in 0.7%C steel with fine pearlite structure, with hardness HV330 (average value of five measurements at random positions, made with a Mitutoyo Vickers hardness tester under a load of 10 N). All tests were conducted with the same maximum contact pressure (0.9 GPa), rolling speed (500 rpm) and sliding/rolling ratio (0.5%). Wet contact was realized by means of a jet of water with the addition of 10% glycol for the prevention of test bench corrosion. In three tests (identified as T1, T2 and T3), dry and wet contact phases of 50,000 cycles each were alternately applied, starting with dry contact. These tests were carried out in the same working condition, in order to ensure a sufficient damage repeatability. In the test identified as T4, 600,000 cycles in dry contact were applied, subsequently wet contact was applied. In the test identified as T5, 10^6 cycles in dry contact were applied, subsequently wet contact was applied. These two tests were carried out without repetitions, in order to explore the trend of the damage occurring when long dry phases are expected. However, regardless of the repetitions, it has to be remarked that the work was mainly addressed at evaluating the correspondence of the measurements to the damage occurring, rather than on the damage itself. The tests were stopped when severe damage occurred on the surface: this condition was identified by a severe increment of the vibrations of the mobile mandrel, as detailed below in the results section. A summary of the applied test conditions in terms of sequence of dry and wet sessions is shown in Table 1.

Figure 2(a) shows a schematic of the vision-based measurement system and Figure 2(b) shows the vision-based measurement system integrated with the test bench. The vision system performs measurements on the fixed wheel specimen. With reference to Figure 2, C is a high-speed camera (PROMON 501; AOS Technologies AG), L1a and L1b are two laser pointers suitably defocused to illuminate the specimen surface for 2D analyses. L2 is a dedicated laser stripe, to perform measurements along the radial direction of the specimen (section profile analysis), whereas L3 is a laser stripe for the measurement of the angular position during the tests, allowing for the synchronization between images and angular position. A f/50 mm lens is used.

A purposely designed encoder was used to measure the angular position of the rolling specimen. This component, shown in Figure 3, is an axial cam, with an external diameter of 50 mm and internal diameter of 44 mm; the height of the region with the maximum diameter varies linearly along the circumference from 3 to 8 mm. Since the encoder is fixed on a disk screwed onto the specimen, the encoder and the specimen roll coaxially. Every time the specimen is disassembled and reassembled, the zero position of the encoder always coincides with the same portion of the specimen. The camera acquires images with dimensions (1280 px × 240 px), with a bit depth of 8 bit, and the resulting field of view (FOV) is (26 mm × 6.5 mm) with spatial resolution equal to 0.021 mm/px, in both *X* and *Y* directions, as defined in Figure 3.

During the dry tests, images of the surface of the wheel specimens were continuously acquired at a frequency of 377 fps. They were acquired with a gain of

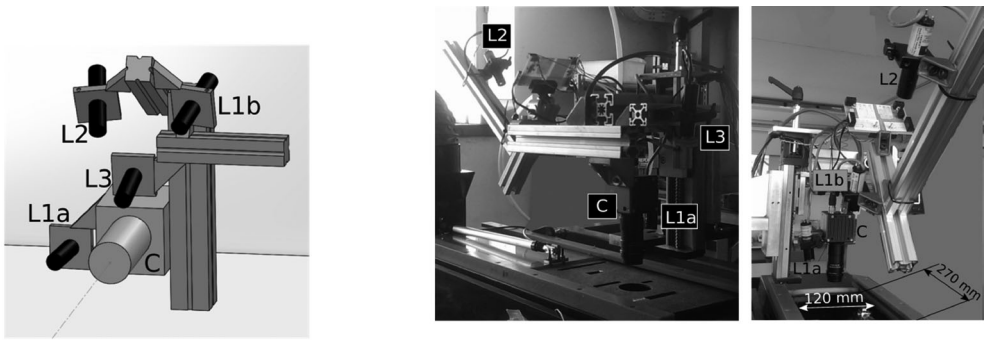

a b

Figure 2. Vision system integrated on the RCF test bench.

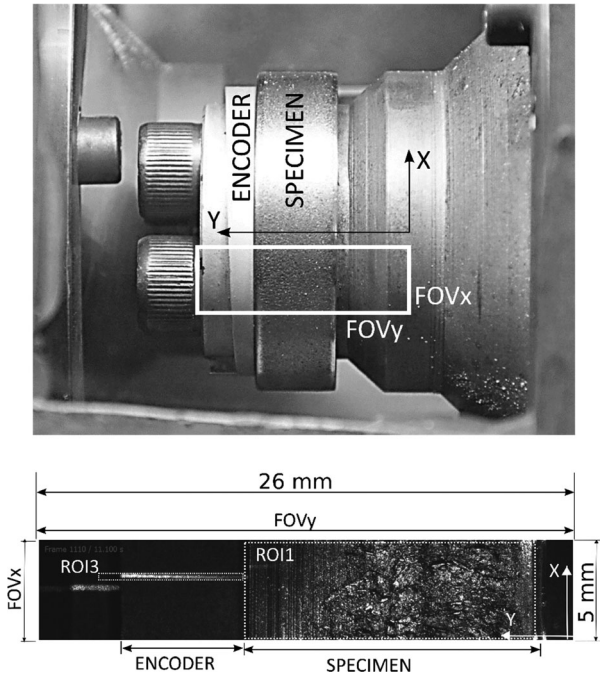

Figure 3. Analogic, linear encoder fixed on a disk coaxially screwed on the specimen. Definition of the *X* and *Y* directions.

24 and an exposure time of 40 µs. In the performed tests, surface images of rolling wheel specimens are acquired every 10 s, each acquisition having a duration of 2 s. Acquisitions are also performed at the beginning and at the end of each step, with the mandrel rotating at the reduced speed of 5 rpm. In these cases, the acquisition frequency of the vision-based measurement system is 100 fps and the duration of the acquisition is 1 min.

3. Image processing

Images of the surface of the specimen undergo simple and fast image processing to quantify surface damage, allowing the definition and assessment of synthetic indexes. Three regions of interest (ROI) were defined, shown in Figure 4. ROI1 includes the surface illuminated by the defocused lasers L1a and L1b; ROI2 includes the region illuminated by laser blade L2; ROI3 includes the region illuminated by laser blade L3.

3.1. Angular position measurement

Laser L3 projects a stripe on the encoder, and the corresponding acquired image of this projection is shown in Figure 4, completely included in ROI3. While the specimen and the encoder are rolling together, the height of the encoder profile linearly varies; therefore, its measurement in each image allows the determination of the angular position of the specimen. As the L3 laser stripe and the corresponding region of interest on the specimen surface are acquired in the same images, the length of the laser stripe included in the ROI3 allows determining the position on the specimen surface of the image acquired in ROI1 and ROI2.

ROI3 is univocally defined on the image before the image processing starts, so that it only contains the projected laser stripe. The portion of image contained in ROI3 undergoes a thresholding at a level of grey of 62.7: this means that the value of pixels with a grey level lower than 62.7 are put equal to zero and the value of pixels with a grey level >62.7 are put equal to one. This way, the resulting image is binary. Such thresholding was chosen to eliminate the grey levels corresponding to a not damaged surface. Details about this procedure are given in [23]. For each column c of the region of interest ROI3, the row position r_G is calculated through the following equation:

$$r_G = \frac{\sum_r l_r \cdot r}{\sum_r r} \tag{1}$$

where l_r is the level of grey of the pixel positioned in column c and row r, and r is the row, once the column is fixed. r_G is a weighted average corresponding to the centroid of the grey levels, so that an array $\{rG\}$ is available. The number of elements of the array is the encoder length.

3.2. Diffused light image analysis (2D analysis)

Lasers L1a and L1b project a diffused light, which results in a scattered light pattern on the specimen surface, whose images exhibit bright areas having number, dimension, position, shape and orientation that can be correlated to the formation of small dips and crests

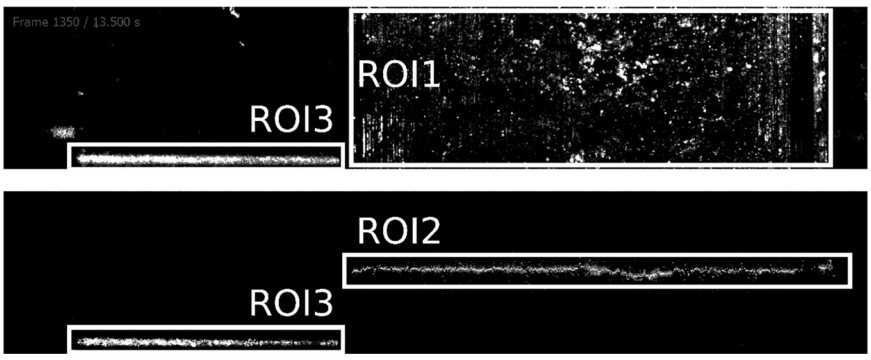

Figure 4. Definition of the regions of interest (ROI).

during wear and RCF processes. In fact, in [23], it is shown that the brighter areas correspond to the bottom of surface pits. To analyse such non-texturized discrete defects, blob analysis is used. Considering an image, a blob is each pixel group within a closed line: in the presented work, blobs correspond to bright areas and, to highlight them, each image underwent first the same thresholding process. Blob analysis allowed deriving a number of parameters, such as the number of blobs, their area and their linear dimensions, e.g. the height and width of the rectangles that circumscribe the blobs [9]. In this work, the first significant parameter is the *R*B, defined as follows:

$$R_B = \frac{A_B}{A_{ROI1}} \tag{2}$$

where A_B is the sum of the areas of the blobs found in the region ROI1, averaged over the whole specimen surface, and A_{ROI1} is the total area of ROI1.

3.3. Profile measurements

The profile of the contact surface along the radial direction was obtained by elaboration of the laser blade track acquired during the tests, with a precision of 0.018 mm. A scheme of the elaboration procedure is shown in Figure 5: the image of the laser blade, deformed by the surface asperities, is calibrated as detailed in [22] in order to obtain the contact surface profile on a radial plane.

4. Results

Each test was stopped when the surface was severely damaged; this condition was identified by a significant increment of the vibrations of the mobile mandrel, exceeding 2 m/s^2. The specimen surface appearance at the end of the test T3 is shown in Figure 6. A marked deformation at the border of the contact surface was clearly visible.

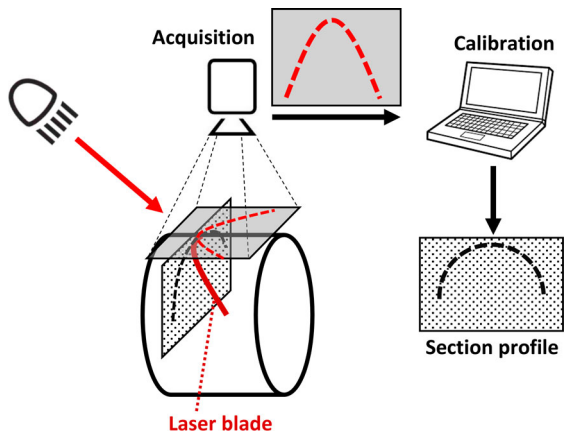

Figure 5. Scheme of laser blade elaboration and section profile reconstruction.

Figure 7 shows the accelerations of the mobile mandrel in the five tests; the grey bands correspond to the phases of wet contact. The acceleration profiles of tests T1, T2 and T3, which were carried out with the alternation of equally lasting dry and wet contact sessions, were characterized by a rather stable band of variation for most of the test duration, until a rapid increment occurred in the final part, clearly related to the occurrence of severe surface damage. Test T4, which was characterized by a long dry session before the application of water, was rather stable for most of the test, but the final raise was even more sudden than in the previous tests. This likely happened because in the final part of the test, once water began to be applied, the mechanism of crack propagation due to the entrapped fluid pressurization started and there were no more dry sessions mitigating it by wear. Test T5, which was characterized by a very long dry session before the application of water, had a very different behaviour: vibrations started to raise progressively but significantly after 200,000 cycles; when water was applied, the sudden increment characterizing the occurrence of severe damage in the previous tests was not observed. This means that severe damage had already occurred in the dry session.

4.1. Two-dimensional image analysis

Figure 8 shows the R_B parameter for all the tests. Filled triangles refer to the measurements after the dry phase, empty dots after the wet one. In the test T1, initially R_B was generally higher after the dry sessions than after

Figure 6. Observed specimen at the end of test T3.

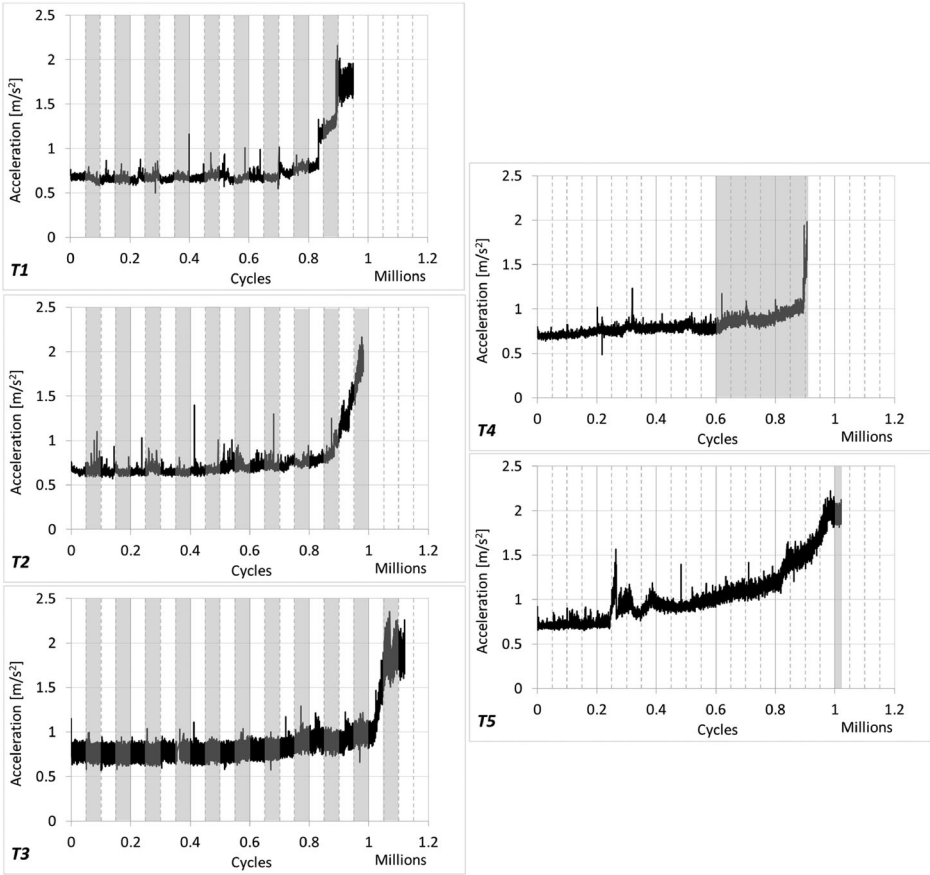

Figure 7. Accelerations of the mobile mandrel during the tests. Grey bands correspond to wet contact sessions.

the wet ones (with some exceptions), meaning that the vision system recognized a more perturbed surface appearance after the formers. This tendency was inverted after 700,000 cycles: indeed, in the final part of the test, R_B was higher after the wet session than after the dry one. A similar behaviour could be observed in the test T2, although the overall values of R_B were lower than in the previous test: this is due to the fact that R_B was averaged over the whole contact surface, whereas in this test, the damage involved a part of it. The tests T3, again, showed a similar behaviour, despite a slight anticipation of the inversion of tendency and generally higher values of R_B, sign of more extended and severe damage. These results can be put in relationship with the damage phenomena occurring at the contact surface, studied in several previous works. In sliding, dry contact ratcheting and wear are the prevailing damage mechanisms, which initially cause plastic flow, corrugations and small surface cracks with a low inclination with respect to the contact surface [10,12]: this explains the increment of R_B after the dry sessions. When water is added, the coefficient of friction lowers and ratcheting arrests [17]; on the contrary, it is probable that local contact between asperities tends to smooth the contact surface, thus explaining the lowering of R_B. However, ratcheting restarts at each dry session, increasing the depth and the slope of the surface cracks; when they are long enough, in the wet sessions, the mechanism of crack propagation due to the entrapped fluid pressurization can be activated [17,20]. When this happens, the effect of the wet and dry sessions on the surface degradation is inverted: wet sessions increase the damage due to crack propagation, whereas dry sessions mitigate this effect by means of wear that, by removing material layers from the surface, reduces the length of the cracks previously propagated [24]. This explains why, after a certain number of cycles, there is an inversion of the tendency of R_B.

In test T4, when water was added after a 600,000 cycles dry session, the R_B raised suddenly. Again, this is consistent with the expected damage phenomena: as the dry session was uninterrupted for a much longer period than in the previous tests, when water was added, the surface cracks were likely long enough for activating the entrapped fluid pressurization mechanism, this way increasing the surface deterioration.

In test T5, which was characterized by a 10^6 cycles long dry session, the R_B value was slightly progressing during the dry session, as highlighted by the trend line; the application of water did not cause a significant variation. The vibrations as well increased progressively in the dry session, with no jumps in the wet phase. This means that the continued application of dry contact for such a high number of cycles induced severe damage even prior to the application of water.

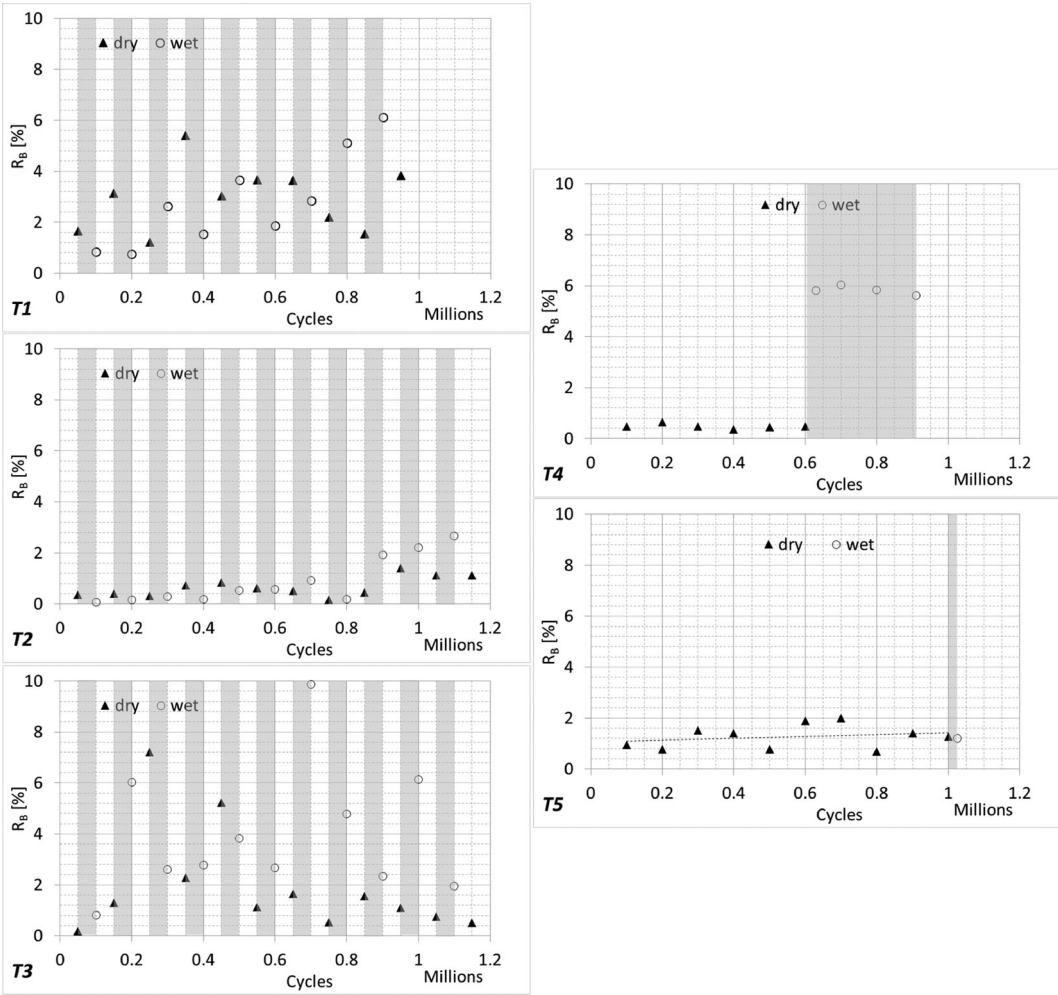

Figure 8. R_B parameter during the tests. Grey bands correspond to wet contact sessions.

According to these results, the main potential of R_B is that it is able to detect when the prevailing damage mechanism changes from ratcheting to fluid-driven crack propagation in frequently alternated dry–wet contact sessions. The occurrence of this change can be identified by the fact that R_B begins to be higher after the wet session than after the dry ones. This is a noticeable result, because the onset of fluid-driven crack propagation can be detected much earlier than it is allowed by the vibration profiles, and the test can be stopped for carrying out the destructive analyses on the specimens when the fatigue failure is at an incipient stage. The main point of weakness of this method is that it is insensitive to localized damage; therefore, the absolute values of R_B cannot be used for comparing the surface state of different specimens: they are effective for reconstructing the evolution of the surface state on the same specimen.

4.2. Section profile analysis

The section profile analysis is able to give information about the surface topology and is particularly effective in analysing the depth and the shape of localized damage. Given the resolution of 18 μm of this system, it can work for analysing defects having larger size, e.g. when they are at the stage of pits or spalls. In this paper, the results of the application of this system at the end of the test T5 are presented; these results are representative of the other tests as well. Three positions were chosen on the contact surface, highlighted in Figure 9, in order to show the variability of the damage that can be observed on the surface. The profiles were taken on the contact surface along the axial direction.

Figure 10 shows the 2D image acquired on the specimen of test T5 in position P_1, the acquired laser blade and the corresponding reconstructed section profile. Note that the width of the acquired profile is about

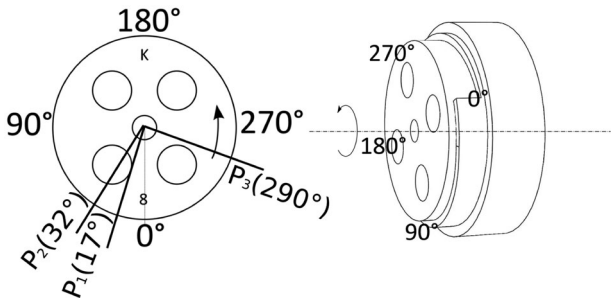

Figure 9. Positions of the 3D image elaboration.

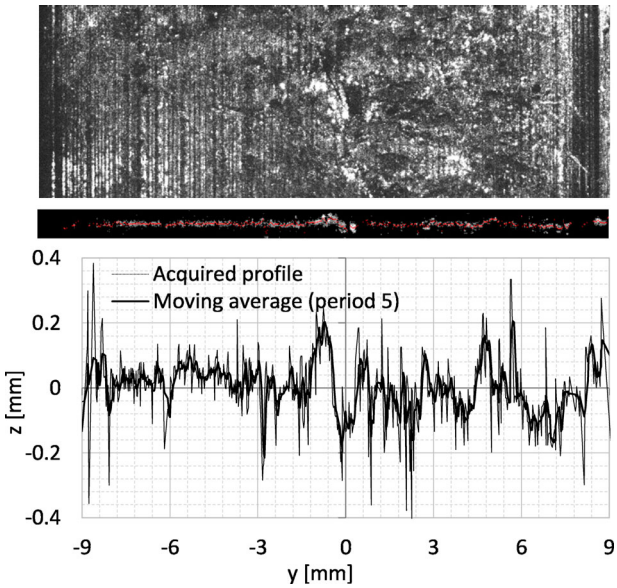

Figure 10. Acquired 2D image, acquired laser blade and section profile reconstruction in the position P_1 of the specimen at the end of the test T5.

18 mm, exceeding the original specimen width due to the plastic deformation of the contact surface borders in the axial direction, as shown in Figure 6. The latter is shown both as it was obtained and after smoothing by a period 5 moving averaging. On the right of the 2D image, a roughened zone is visible; this zone was detected by the curvature of the laser blade, and the reconstructed profile allowed estimating the depth of the marks, which is about 0.4 mm from peak to valley.

Figure 11 shows the same results for position P_2. In this case, a localized damage (spall) is visible in the central zone of the contact patch on the 2D image. The section profile analysis detected this spall and allowed estimating its depth as 0.6 mm.

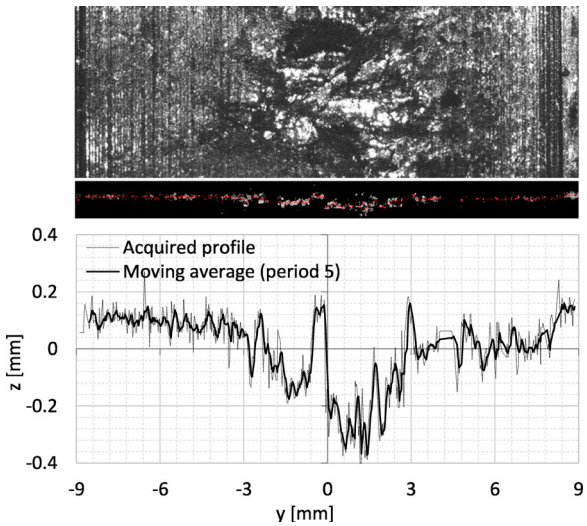

Figure 11. Acquired 2D image, acquired laser blade and section profile reconstruction in the position P_2 of the specimen at the end of the test T5.

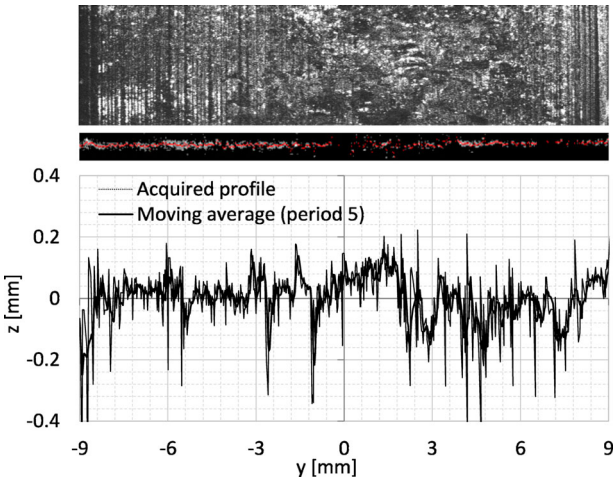

Figure 12. Acquired 2D image, acquired laser blade and section profile reconstruction in the position P_3 of the specimen at the end of the test T5.

Figure 12 shows the profile acquired in position P_3: similar to position P_1, the damage was more diffused along the width than it is in position P_2; a more perturbed region can be identified on the right side of the surface, with a maximum peak-to-valley distance of about 0.4 mm.

Figure 13 shows the assembly of the acquired profiles along the whole contact surface of the T5 test specimen. This image shows a more damaged strip on the right-hand side of the contact surface, in agreement with the appearance of the acquired images. Despite the fact that this technique still needs refinement, especially in the smoothing and resolution along the angular direction, this image shows the potential of the radial section reconstruction as a tool for contactless 3D surface topology analysis.

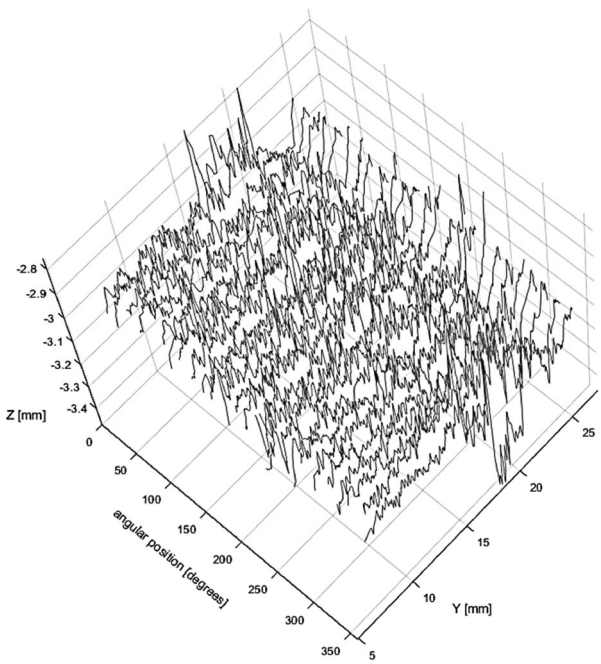

Figure 13. Assembly of reconstructed profiles of test T5.

5. Discussion

The results of these experiments show the potential of the vision technology and image analysis as a monitoring and measurement tool that can integrate usual systems used for controlling rolling contact tests. In particular, the proposed 2D analysis technique showed its ability of detecting the onset of fluid-driven crack propagation before vibration analysis can. The final failure, which is detected by the increment of vibrations of the mobile mandrel, becomes evident just in the final cycles; however, the analysis of the R_B parameter suggests that fluid-driven RCF starts earlier, becoming unstable just in the final cycles. Indeed, vibrations are sensitive to the overall contact elasticity, which changes significantly only when the damage becomes severe. On the contrary, R_B is sensitive to the surface state and is able to capture changes even when the damage involves a small depth below the surface. However, R_B alone is not effective in determining the damage severity: being determined by a surface analysis, no information about the damage depth is provided. Furthermore, being obtained by an averaging process over the whole contact surface, it can provide wrong information when the failure is determined, for instance, by a local large spall.

The lack of the 2D analyses can be compensated for by the section profile analysis, which was shown to be effective particularly in detecting and analysing large spalls and other severe perturbations of the surface smoothness. Being synchronous with the system for determining the angular position, this system can be used for monitoring the growth of such defects. Furthermore, despite refinements are still needed, this system can be used for the overall reconstruction of the surface topology.

The limitation of both vision techniques is that during wet sessions, they cannot be used online: in fact, due to the water splashes, the camera needs to be protected and cannot work. As large spalls can develop rapidly during wet session, the vibration monitoring system still is needed as a diagnostic tool for detecting the final failure.

Another limitation is that these methods, giving information on the surface state, do not allow evaluation of hidden phenomena, such as crack propagation in the subsurface layer. For improving the damage monitoring, further measurement systems, able to detect subsurface crack propagation, are under study.

6. Conclusions

A vision-based system was set up for monitoring the evolution of the specimen surface during rolling contact tests. It provides information by means of 2D analysis of images of the specimen surface acquired under defocused laser illumination, and by analysis of the images of a laser blade deformed by surface asperities (section profile analysis). Synthetic indexes were defined for quantifying the damage obtained by the 2D analysis. This system was applied to alternated dry–wet tests on railway wheel steels.

The 2D image analysis was shown to be able to provide information about the starting of fluid-driven RCF; the section profile analysis was shown to be able to provide a quantitative estimation of the damage depth. Furthermore, it appeared a promising tool for 3D surface topology reconstruction. Overall, the vision system appears a useful tool for providing quantitative information about the damage evolution in rolling contact tests, being able to identify different damage mechanisms and to localize their occurrence in space and time.

This experience showed that a monitoring system integrating different measurement and diagnostic tools, including vibration and image analysis, can be a very effective tool for controlling the evolution of damage in rolling contact tests.

Disclosure statement

No potential conflict of interest was reported by the author(s).

ORCID

Ileana Bodini http://orcid.org/0000-0003-4904-2044
Candida Petrogalli http://orcid.org/0000-0002-1774-3914
Angelo Mazzù http://orcid.org/0000-0002-6074-3143
Simone Pasinetti http://orcid.org/0000-0002-5098-6395

References

[1] Bruce T, Long H, Dwyer-Joyce RS. Threshold maps for inclusion-initiated micro-cracks and white etching areas in bearing steel: the role of impact loading and surface sliding. Tribol Lett. 2018;66(3):211.
[2] Savolainen M, Lehtovaara A. An approach to investigating subsurface fatigue in a rolling/sliding contact. Int J Fatigue. 2018;117:180–188.
[3] Dimkovski Z, Lööf PJ, Rosén BG, et al. Functional parameter screening for predicting durability of rolling sliding contacts with different surface finishes. Surf Topogr Metrology and Properties. 2018;6:024005.
[4] Gutiérrez Guzmán F, Oezel M, Jacobs G, et al. Reproduction of white etching cracks under rolling contact loading on thrust bearing and two-disc test rigs. Wear. 2017;390-391:23–32.
[5] Wei J, Zhang AQ, Gao P. A study of spur gear pitting under EHL conditions: theoretical analysis and experiments. Tribol Int. 2016;94:146–154.
[6] Donzella G, Faccoli M, Mazzù A, et al. Influence of inclusion content on rolling contact fatigue in a gear steel: experimental analysis and predictive modelling. Eng Fract Mech. 2011;78(16):2761–2774.
[7] Shebani A, Iwnicki S. Prediction of wheel and rail wear under different contact conditions using artificial neural networks. Wear. 2018;406–407:173–184.

[8] Huang YB, Shi LB, Zhao XJ, et al. On the formation and damage mechanism of rolling contact fatigue surface cracks of wheel/rail under the dry condition. Wear. 2018;400–401:62–73.
[9] Maya-Johnson S, Santa JF, Toro A. Dry and lubricated wear of rail steel under rolling contact fatigue – wear mechanisms and crack growth. Wear. 2017;380–381:240–250.
[10] Faccoli M, Petrogalli C, Lancini M, et al. Rolling contact fatigue and wear behavior of high-performance railway wheel steels under various rolling-sliding contact conditions. J Mater Eng Perform. 2017;26(7):3271–3284.
[11] Wang WJ, Lewis R, Yang B, et al. Wear and damage transitions of wheel and rail materials under various contact conditions. Wear. 2016;362–363:146–152.
[12] Mazzù A, Petrogalli C, Faccoli M. An integrated model for competitive damage mechanisms assessment in railway wheel steels. Wear. 2015;322–323:181–191.
[13] Donzella G, Faccoli M, Mazzù A, et al. Progressive damage assessment in the near-surface layer of railway wheel-rail couple under cyclic contact. Wear. 2011;271:408–416.
[14] Faccoli M, Petrogalli C, Lancini M, et al. Effect of desert sand on wear and rolling contact fatigue behaviour of various railway wheel steels. Wear. 2018;396–397:146–161.
[15] Zhu Y, Yang HY, Wang WJ. Twin-disc tests of iron oxides in dry and wet wheel-rail contacts. Proc Inst Mech Eng Part F – J Rail Rapid Transit. 2016;230(4):1066–1076.
[16] Omasta M, Machatka M, Smejkal D, et al. Influence of sanding parameters on adhesion recovery in contaminated wheel–rail contact. Wear. 2015;322–323:218–225.
[17] Mazzù A, Petrogalli C, Lancini M, et al. Effect of wear on surface crack propagation in rail-wheel wet contact. J Mater Eng Perform. 2018;27(2):630–639.
[18] Shi LB, Ma L, Guo J, et al. Influence of low temperature environment on the adhesion characteristics of wheel-rail contact. Tribol Int. 2018;127:59–68.
[19] Hardwick C, Lewis R, Stock R. The effects of friction management materials on rail with pre existing RCF surface damage. Wear. 2017;384–385:50–60.
[20] Makino T, Kato T, Hirakawa K. The effect of slip ratio on the rolling contact fatigue property of railway wheel steel. Int J Fatigue. 2012;36(1):68–79.
[21] Mazzù A, Solazzi L, Lancini M, et al. An experimental procedure for surface damage assessment in railway wheel and rails steels. Wear. 2015;342–343:22–32.
[22] Bodini I, Sansoni G, Lancini M, et al. A novel optical apparatus for the study of rolling contact wear/fatigue based on a high speed camera and multiple-source laser illumination. Rev Sci Instrum. 2016;87(8).
[23] Bodini I, Petrogalli C, Faccoli M, et al. Evaluation of wear in rolling contact tests by means of 2D image analysis. Wear. 2018;400–401:156–168.
[24] Faccoli M, Petrogalli C, Lancini M, et al. Rolling contact fatigue and wear behaviour of high-performance railway wheel steels under various rolling-sliding contact conditions. J Mater Eng Perform. 2017;26(7):3271–3284.